applied sciences

MDPI

*Article*

# Channel Estimation Based on IOTA Filter in OFDM/OQPSK and OFDM/OQAM Systems

**Xiao Zhou, Chengyou Wang * and Ruiguang Tang**

School of Mechanical, Electrical and Information Engineering, Shandong University, Weihai 264209, China; zhouxiao@sdu.edu.cn (X.Z.); trg@mail.sdu.edu.cn (R.T.)

* Correspondence: wangchengyou@sdu.edu.cn; Tel.: +86-631-568-8338

Received: 31 December 2018; Accepted: 1 April 2019; Published: 7 April 2019


**Featured Application: This channel estimation method can be utilized to improve the underwater acoustic communication and fifth-generation (5G) wireless communication systems.**

**Abstract:** In this paper, we present a study of bit error rate (BER) for orthogonal frequency division multiplexing/offset quadrature phase shift keying (OFDM/OQPSK) and OFDM/offset quadrature amplitude modulation (OQAM) systems with an isotropic orthogonal transfer algorithm (IOTA) filter. The novel noise suppression method based on an IOTA filter is proposed to reduce the error of channel estimation caused by additive white Gaussian noise (AWGN). The OFDM/OQPSK and OFDM/OQAM systems do not insert the guard interval (GI) and pilots in the signal frames, thus they possess transmission efficiency. An analysis was carried out for convolutional coded OFDM/OQPSK and OFDM/OQAM systems in Rayleigh fading channels with generator polynomials and constraint lengths. Compared with conventional OFDM/QPSK and OFDM/QAM systems with the insertion of comb-type pilots, the proposed IOTA filter-based channel estimation method can provide significant energy per bit to time-varying noise power spectral density ratio gains over time and frequency-selective propagation Rayleigh fading channels in OFDM/OQPSK and OFDM/OQAM systems.

**Keywords:** channel estimation; orthogonal frequency division multiplexing (OFDM); isotropic orthogonal transform algorithm (IOTA); offset quadrature phase shift keying (OQPSK); offset quadrature amplitude modulation (OQAM); additive white Gaussian noise (AWGN)

## 1. Introduction

Wavelets have been a very hot research area in recent years. Their application ranges from function approximation, signal multiresolution representation, and image compression to signal processing and other fields. The popularity of wavelets is primarily due to their interesting structures, which can provide perfect time-frequency localization (TFL) characteristics. A few investigators have begun to exploit these time-domain and frequency-domain features of wavelets for application in wireless communication systems [1–3].

In classical orthogonal frequency division multiplexing (OFDM) systems, a guard interval (GI) is inserted in front of OFDM symbols to effectively combat the multipath effect with little loss of spectral efficiency. It is robust to inter-symbol interference (ISI), but sensitive to inter-carrier interference (ICI) due to Doppler spread in the frequency domain. Offset quadrature phase shift keying (OQPSK) and offset quadrature amplitude modulation (OQAM) are spectrally efficient modulation schemes which are alternative technologies for replacing QPSK and QAM. OQPSK and OQAM modulations possess good TFL properties by utilizing an isotropic orthogonal transfer algorithm (IOTA) filter. The polyphase IOTA filters are utilized as both transmit and receive filters to enhance robustness for channel delay

and Doppler spread. In OFDM/OQPSK and OFDM/OQAM systems, the orthogonal condition of the subcarriers is guaranteed from the complex domain to the real domain. Thus, the GI inserted between consecutive OFDM signal frames can be removed in OFDM/OQPSK and OFDM/OQAM systems. The ISI and ICI in OFDM/QPSK systems can be suppressed utilizing polyphase filter banks with good TFL property. Compared with OFDM systems, the TFL property of the IOTA filter can guarantee good bit error rate (BER) performance that combats ISI and ICI in OFDM/OQPSK and OFDM/OQAM systems.

This paper proposes a channel estimation method based on an IOTA filter, which is applied in OFDM/OQPSK and OFDM/OQAM systems. It has high spectral and data transmission efficiency which effectively suppresses the additive white Gaussian noise (AWGN) existing at the estimated channel coefficients in the time domain. It can improve the system's BER and normalized minimum square error (NMSE) performance, and is easy to implement in hardware. Simulation results verified that the proposed IOTA filter channel estimation method was superior to the conventional comb-type pilots insertion based least square (LS) method in terms of BER and NMSE performance under Rayleigh fading channel conditions.

The remainder of this paper is organized as follows. In Sections 2 and 3, the related work and OFDM/OQPSK system model are presented. Section 4 introduces the channel coding. Section 5 illustrates the simulation results. Conclusions are presented in Section 6.

## 2. Related Work

Recently, many experiments and theoretical analyses of OFDM-IOTA systems have been proposed. A new pilot and preamble structure for the channel estimation appropriate for the OFDM/OQAM system was proposed. A limitation of the paper was that it was implemented in an uncoded OFDM system [4]. Although a comparison of cyclic prefix (CP)-OFDM with OFDM-IOTA under a typical system was proposed, the disadvantage of the system was the existence of frequency offset error at the receiver [5]. A hardware architecture of the pulse shaping filter used in multicarrier systems was proposed in [6]. IOTA pulse shaping filters were used to reduce hardware overhead in multicarrier systems based on faster-than-Nyquist (FTN) signaling. The IOTA filter has an overhead of 28% in silicon area compared with the FTN iterative decoder. The disadvantage is that the high complexity of the hardware mapped architecture. A multiple-input multiple-output (MIMO)-IOTA system was proposed in [7], and the MIMO-IOTA system achieved better performance compared with an OFDM system at low-to-medium signal-to-noise ratios (SNRs). Raised cosine, IOTA, Hermite, and Gaussian wavelets were proposed in [8]. The BER results of the IOTA method were better than those of the square function method and slightly worse than the Hermite function method. As the SNR increased, the Hermite filter showed the best BER performance compared with IOTA and square filters. The disadvantage of the Hermite filter is that it only concentrates on ICI suppression and does not consider the effect of different types of multipath in the simulation results. The capacity of OFDM/OQAM systems with IOTA filters was evaluated through information theoretical analysis in [9]. The promising results motivate further research on the utilization of the intrinsic interference in order to explore the potential to attain maximum performance gain in future OFDM/OQAM systems. OFDM/OQAM systems showed significant spectral efficiency while compared with CP-OFDM systems.

In [10], the BER performance of OFDM interleave division multiple access (IDMA) with wavelet families, such as Haar, Daubechies, and Symlets, was compared over an AWGN channel. The Daubechies wavelet has the best BER performance under 16-quadrature amplitude modulation (16-QAM). The circular 16-QAM constellation has been derived and applied in Fourier- and wavelet-based OFDM systems [11]. The circular scheme showed slightly better BER performance than the square scheme. The reason is that the power consumption of the circular constellation signals is less than that of the square scheme. To maximize the system capacity, the filter-bank-based multicarrier (FBMC) scheme provides higher capacity performance compared with the OFDM system [12]. In contrast to the OFDM system, the FBMC waveform has been demonstrated to be

less sensitive to timing error between the different cells, due to the better frequency localization of the prototype filter. A new OFDM system based on a discrete cosine harmonic wavelet transform (DCHWT) for binary phase shift keying (BPSK) and QPSK signals was proposed in [13]. The proposed DCHWT-OFDM system provided superior performance in terms of BER and peak-to-average power ratio (PAPR) compared with the discrete cosine transform (DCT)-OFDM, discrete Fourier transform (DFT)-OFDM, and Haar WT-OFDM systems. However, the DCHWT-OFDM and Haar WT-OFDM systems may not have significant BER improvements under 16-QAM and 64-QAM signal constellation.

## 3. OFDM/OQPSK System Model

### *3.1. OFDM/OQPSK Symbols*

Figure 1 represents the real and imaginary values of OFDM/OQPSK symbols. The green triangle signature represents the OFDM/QPSK symbols in conventional CP-OFDM systems. The classical OFDM/QPSK symbols are real mapped into two parts (i.e., real and imaginary values in the OFDM/OQPSK-IOTA system), which are located in four quadrants. In Figure 1, the circular yellow signature represents the real value of OFDM/OQPSK symbols and the blue signature represents the imaginary value of OFDM/OQPSK symbols. $\tau_0$ and $v_0$ are the time-domain duration and frequency-domain spacing for OFDM/OQPSK symbols, respectively. $\tau_0$ equals to half of the OFDM/QPSK symbol duration $T_s$, that is, $\tau_0 = T_s/2$. The phases and dephases of the real and imaginary values of OFDM/OQPSK symbols are represented as $j^{m+n}$ and $j^{-(m+n)}$, respectively. If $(m+n)\%4 = 0$, then $j^{m+n} = 1$, $j^{-(m+n)} = 1$; if $(m+n)\%4 = 1$, then $j^{m+n} = j$, $j^{-(m+n)} = -j$; if $(m+n)\%4 = 2$, then $j^{m+n} = -1$, $j^{-(m+n)} = -1$; if $(m+n)\%4 = 3$, then $j^{m+n} = -j$, $j^{-(m+n)} = j$; where % is the modulo operation.

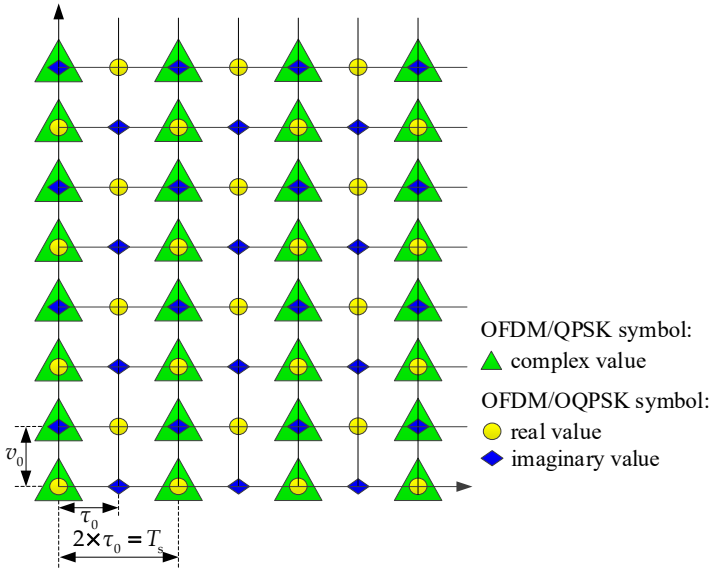


**Figure 1.** Real and imaginary values of orthogonal frequency division multiplexing (OFDM)/offset quadrature phase shift keying (OQPSK) symbols.

### *3.2. Design of the IOTA Filter*

The approximate time-domain IOTA function, which is denoted as $\xi_{\tau_0}(t)$, can be expressed as [14]:

$$\xi_{\tau_0}(t) = \frac{1}{2}\sum_{k=0}^{K-1}\left\{\bar{d}_{k,v_0}\left[h_{\mathrm{EGF}}(t+\frac{k}{v_0}) + h_{\mathrm{EGF}}(t-\frac{k}{v_0})\right]\right\}\cdot\sum_{l=0}^{K-1}\left[\bar{d}_{l,\tau_0}\cos(2\pi l\frac{t}{\tau_0})\right], -4\tau_0 \le t \le 4\tau_0, \quad (1)$$

where $t$ is the time and $k$ represents the number of subcarriers. $h_{\mathrm{EGF}}(t) = 2^{\frac{1}{4}} \mathrm{e}^{-\pi t^2}$ is the extended Gaussian filter (EGF) in the time domain. Normally, $\tau_0$ and $v_0$ are chosen to be $1/\sqrt{2}$ to maintain the orthogonality characteristics between consecutive OFDM symbols in the time domain and adjacent subcarriers in the frequency domain. When $\tau_0 = v_0 = 1/\sqrt{2}$, $t \in [-2\sqrt{2}, 2\sqrt{2}]$. The polyphase IOTA filter puts the IOTA values into the IOTA buffer with the length equals to half of the fast Fourier transform (FFT) size and the width equals to 8. The IOTA coefficients $\bar{d}_{k,v_0}$ can be expressed as:

$$\bar{d}_{k,v_0} = \sum_{q=0}^{Q-1} b_{k,q} \cdot \mathrm{e}^{-\pi(2q+k)}, 0 \le k \le K-1, 0 \le q \le Q-1, \tag{2}$$

where $K$ and $Q$, which are integer numbers, are two parameters of the IOTA filter. In general, $K = 15$ and $Q = 8$ are chosen in IOTA filter design [14]. Table 1 represents a list of $b_{k,q}$ coefficients.

**Table 1.** $b_{k,q}$ coefficients of the isotropic orthogonal transfer algorithm (IOTA) filter.

| $k$ | $q$=0 | $q$=1 | $q$=2 | $q$=3 | $q$=4 | $q$=5 | $q$=6 | $q$=7 |
|---|---|---|---|---|---|---|---|---|
| 0 | 1 | 0.75 | 1.6406 | 2.6367 | 4.6529 | 6.9749 | 11.5368 | 16.8193 |
| 1 | −1 | −1.875 | −3.4219 | −5.9131 | −9.8831 | −15.7769 | −24.8536 | 0 |
| 2 | 0.75 | 1.1875 | 3.0176 | 4.7681 | 9.0985 | 14.0379 | 23.4937 | 0 |
| 3 | −0.625 | −0.9609 | −2.2354 | −4.2567 | −7.3957 | −12.2028 | 0 | 0 |
| 4 | 0.5469 | 0.8320 | 1.9036 | 3.4279 | 6.6095 | 10.3934 | 0 | 0 |
| 5 | −0.4922 | −0.7451 | −1.6937 | −3.0167 | −5.6268 | 0 | 0 | 0 |
| 6 | 0.4512 | 0.6812 | 1.5433 | 2.7365 | 5.0687 | 0 | 0 | 0 |
| 7 | −0.4189 | −0.6314 | −1.4279 | −2.526 | 0 | 0 | 0 | 0 |
| 8 | 0.3928 | 0.5913 | 1.3356 | 2.3594 | 0 | 0 | 0 | 0 |
| 9 | −0.3709 | −0.558 | −1.2594 | 0 | 0 | 0 | 0 | 0 |
| 10 | 0.3524 | 0.5299 | 1.1951 | 0 | 0 | 0 | 0 | 0 |
| 11 | −0.3364 | −0.5056 | 0 | 0 | 0 | 0 | 0 | 0 |
| 12 | 0.3224 | 0.4843 | 0 | 0 | 0 | 0 | 0 | 0 |
| 13 | −0.31 | 0 | 0 | 0 | 0 | 0 | 0 | 0 |
| 14 | 0.2989 | 0 | 0 | 0 | 0 | 0 | 0 | 0 |

Table 2 represents a list of important parameters in the IOTA filter, where $k$, $l$, and $q$ are set to be integers. The accuracy of IOTA filter design can reach $0.79 \times 10^{-19}$ [14]. The IOTA filter which is utilized in OFDM/OQPSK and OFDM/OQAM systems increases the accuracy of channel estimation.

**Table 2.** Important parameters in the IOTA filter.

| Parameters | Specifications |
|---|---|
| $\tau_0$ | $1/\sqrt{2}$ |
| $v_0$ | $1/\sqrt{2}$ |
| $t$ | $[-2\sqrt{2}, 2\sqrt{2}]$ |
| $K$ | 15 |
| $Q$ | 8 |
| $k$ | $[0, 14]$ |
| $l$ | $[0, 14]$ |
| $q$ | $[0, 7]$ |

The simulation results of linear and decibel formats of the IOTA filter are represented in Figure 2a,b. When the number of OFDM symbols is $t = 0$, the magnitude of the IOTA filter is equal to 1. The IOTA filter is orthogonal between consecutive OFDM symbols, thus it can efficiently reduce the ISI and ICI.

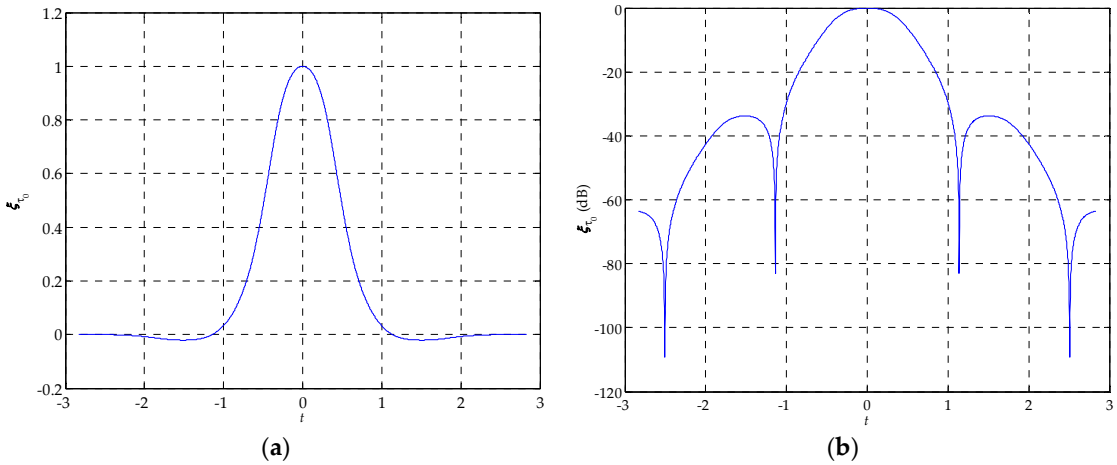


**Figure 2.** IOTA filter in linear and decibel formats: (**a**) Linear format, (**b**) Decibel format.

### *3.3. OFDM-IOTA System Model*

Figure 3 represents the OFDM-IOTA system model. The incoming binary bits are first QPSK modulated, then every OFDM/QPSK symbol is separated into real and imaginary parts, which is called real map. After real mapping, the OFDM symbols are symbol-phased by multiplying them with the phase coefficient $\mathrm{j}^{m+n}$. At the receiver, the OFDM symbols are symbol-dephased by multiplying them with the phase coefficient $\mathrm{j}^{-(m+n)}$. After inverse fast Fourier transform (IFFT) operation, the signals are convoluted by the polyphaser IOTA filter, which can be denoted as $\xi_{\tau_0}(m)$. The transmitted OFDM/OQPSK signals in the time domain can be written as [15]:

$$s^i_{m,n} = \sum_{m=0}^{M-1} \sum_{n=0}^{N-1} a^i_{m,n} \cdot \mathrm{j}^{m+n} \cdot \xi_{\tau_0}(m - n\tau_0) \cdot \mathrm{e}^{\frac{\mathrm{j}2\pi mn}{N}}, 0 \le m \le M-1, 0 \le n \le N-1, \quad (3)$$

where $a^i_{m,n}$ is the real or imaginary OQPSK symbol of the $i$-th signal frame on the $m$-th symbol of the $n$-th subcarrier. $N$ is the number of subcarriers within one OFDM symbol and $M$ is the number of transmitted OFDM/OQPSK symbols. In the OFDM-IOTA system, $M = 300$ and $N = 512$. $\xi_{\tau_0}(m)$ is the transmit IOTA filter on the $m$-th OFDM/OQPSK symbol, and $\tau_0$ is the duration of the OFDM/OQPSK symbol.

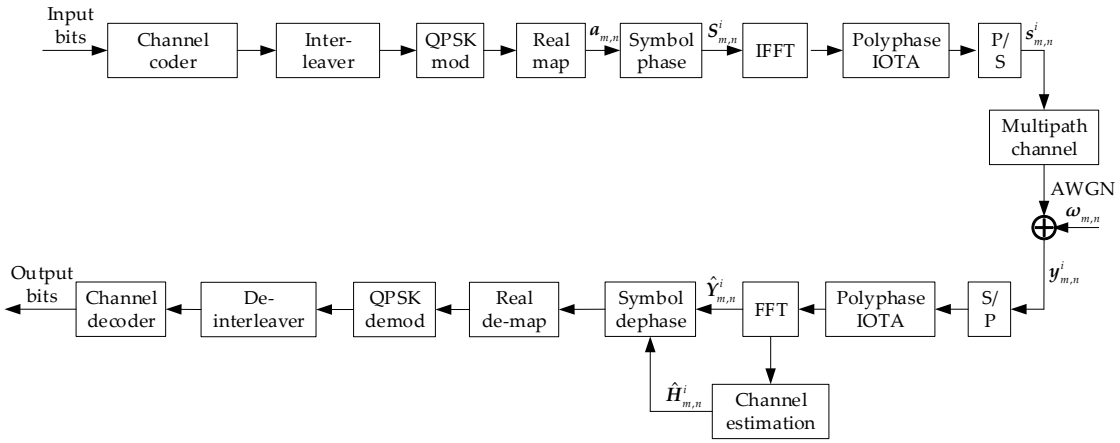


**Figure 3.** OFDM-IOTA system model. AWGN: additive white Gaussian noise; FFT: fast Fourier transform; IFFT: inverse FFT.

Take the $i$-th signal frame for example, suppose $S^i_{m,n}$ to be the FFT of $s^i_{m,n}$, the received frequency-domain symbols after multipath channel $Y^i_{m,n}$ can be represented as:

$$Y^i_{m,n} = S^i_{m,n} \cdot H^i_{m,n} + W^i_{m,n}, \tag{4}$$

where $H^i_{m,n}$ and $W^i_{m,n}$ are the channel frequency response (CFR) and the frequency-domain noise of the $i$-th frame, respectively. After AWGN channel, the received time-domain symbols of the $i$-th frame on the $m$-th symbol and the $n$-th subcarrier can be denoted as $y^i_{m,n}$, which is an IFFT of $Y^i_{m,n}$. The OFDM signals are dephased by multiplying them with the coefficients $\mathrm{j}^{-(m+n)}$. After real de-mapping, the received OFDM/OQPSK signals can be represented as [15]:

$$\hat{Y}^i_{m,n} = \sum_{m=0}^{M-1} \sum_{n=0}^{N-1} y^i_{m,n} \cdot \xi_{\tau_0}(m - n\tau_0) \cdot \mathrm{e}^{\frac{-\mathrm{j}2\pi mn}{N}} + \omega^i_{m,n}, \tag{5}$$

where $\xi_{\tau_0}(m)$ is the receive IOTA filter. $\omega^i_{m,n}$ is the time-domain AWGN of the $i$-th signal frame on the $m$-th symbol of the $n$-th subcarrier. As illustrated in Figure 3, the received OFDM/OQPSK symbols of the $i$-th frame $\hat{y}^i_{m,n}$ are QPSK demodulated, de-interleaved, and finally channel decoded into binary bits [16].

Suppose the FFT transform of $\hat{y}^i_{m,n}$ is $\hat{Y}^i_{m,n}$, after the polyphaser IOTA filter, the estimated CFR $\hat{H}^i_{m,n}$ of the $i$-th frame can be expressed as:

$$\hat{H}^i_{m,n} = 1.4 \cdot \hat{Y}^i_{m,n} \cdot \mathrm{j}^{-(m+n)} / X^i_{\mathrm{P}} + \hat{W}^i_{m,n}, \tag{6}$$

where $X^i_{\mathrm{P}}$ are the preamble symbols of the $i$-th OFDM signal frame. $\hat{W}^i_{m,n}$ is the frequency-domain AWGN in $\hat{H}^i_{m,n}$.

Supposing $\hat{h}_{m,n}$ is the IFFT transform of $\hat{H}^i_{m,n}$, since the noise suppression process will not be carried out in the LS criterion, it degrades the estimation accuracy of channel impulse responses (CIRs). In practice, the OFDM/OQPSK system utilizes an improved minimum mean square error (IMMSE) method to suppress the noise impact on the initial CIR estimation, and the estimated CIR $\widetilde{h}_{m,n}$ is expressed as [16]:

$$\widetilde{h}_{m,n} = \frac{\hat{h}_{m,n} \cdot |\hat{h}_{m,n}|^2}{\alpha \cdot |\hat{h}_{m,n}|^2 + (1-\alpha) \cdot A_i^2}, \tag{7}$$

where $A_i = \max\limits_{0 \le n \le N-1} (|\hat{h}_{m,n}|)$ denotes the maximum amplitude, and $\alpha$ denotes the suppression factor. In practice, $\alpha$ can be chosen in the range of $(0.99, 1)$ according to different modulation modes which are accommodated for $E_\mathrm{b}/N_0$ environments.

Supposing $\widetilde{H}_{m,n}$ is the FFT transform of $\widetilde{h}_{m,n}$, $\hat{R}^i_{m,n}$ is the real value of the $\hat{Y}^i_{m,n}$, the received OFDM/OQPSK symbols of the $i$-th frame $\hat{X}^i_{m,n}$ can be obtained based on LS method:

$$\hat{X}^i_{m,n} = 1.4 \cdot \hat{Y}^i_{m,n} \cdot \mathrm{j}^{-(m+n)} / \widetilde{H}_{m,n}. \tag{8}$$

## 4. Channel Coding

### *4.1. Time Diversity in Jakes Model*

For time diversity, channel coding plus inter-leaver can be used in the time domain. However, to make the technique effective, the time frame has to be greater than the channel coherence time. In this work, we consider a frequency-selective environment and adopt a Rayleigh fading channel model to simulate the time diversity. Subcarriers in different OFDM symbols are considered to fade independently, and subcarriers in the same OFDM symbol experience identical fades. In the time domain, we use the Jakes model to simulate different fading rates, generating a different time diversity

environment. Table 3 represents the main simulation parameters for OFDM/OQPSK, OFDM/QPSK, OFDM/OQAM, and OFDM/QAM systems. The signal modulation patterns are OQAM, QAM, OQPSK, and QPSK, respectively. The symbol rate is 12 kbit/s, the length of FFT is 512, and the carrier frequency is 2 GHz. The fast fading model is the Jakes spectrum and the channel coding is a convolutional encoder with a code rate of 1/2. The inter-leaver is a block inter-leaver with 300 OFDM symbols. The channel decoding algorithm in the systems is Viterbi decoding.

**Table 3.** Main simulation parameters in this paper.

| Parameters | Specifications |
|---|---|
| Symbol duration $T_s$ | QPSK: 1/6000 s, 16-QAM: 1/3000 s |
| Symbol rate | 12 kbit/s |
| Guard interval (GI) length | OFDM-IOTA: 0, CP-OFDM: 128 symbols |
| System model | OFDM-IOTA / CP-OFDM |
| The length of FFT | 512 |
| Carrier frequency | 2 GHz |
| Fast fading model | Jakes spectrum |
| Number of multi-paths | 6 |
| Code rate | 1/2 |
| $\alpha$ | 0.995 |
| Inter-leaver | Block inter-leaver (300 OFDM symbols) |
| Doppler spread | 20, 40, 60, 80 Hz |

### 4.2. Convolutional Encoder and Viterbi Decoder

In OFDM systems, the most widely used channel coding types are block codes and convolutional codes. Convolutional codes have memory, unlike block codes, which provides output using past information bits. If the number of registers is 6, then the constraint length equals to 7 [17,18]. The convolutional encoder consists of a code rate of 1/2, memory of 6, with code generator polynomials 133 and 171 in octal format [17,18]. The convolutional encoder can improve the accuracy of channel estimation for the receivers in both OFDM-IOTA and CP-OFDM systems.

The Viterbi algorithm operates by computing a metric for every possible path in the trellis [13]. The path with the lower metric is retained and the other path is discarded. This process is repeated until the algorithm completes its forward search through the trellis and reaches the termination node, and finally makes a decision on maximum likelihood path. The sequence symbols associate with the path are then released to the destination as the Viterbi decoder output. The Viterbi decoder algorithm can find the lowest Hamming distance to demodulate the input binary bits correctly.

## 5. Simulation Results

### 5.1. The Performance of the OFDM/OQPSK System

Figure 4 represents BER performance over Rayleigh fading channels with different Doppler spread [18]. At the target BER of $10^{-3}$, the IOTA filter channel estimation method under Doppler spread 20 Hz outperforms the IOTA channel estimation method under Doppler spread of 40, 60, and 80 Hz by about 0.4, 5.5, and 9.7 dB $E_b/N_0$ gains. At the target BER of $2 \times 10^{-4}$, under the Doppler spread of 20 Hz, the ideal channel estimation (ICE) method outperforms the IOTA channel estimation method under Doppler spread of 40, 60, and 80 Hz by about 0.4, 6.0, and 9.8 dB $E_b/N_0$ gains. The reason is that when the channel is under fast mobile velocity, the Rayleigh channel is under the condition of severe frequency selectivity, and thereby it causes large amounts of bit errors.

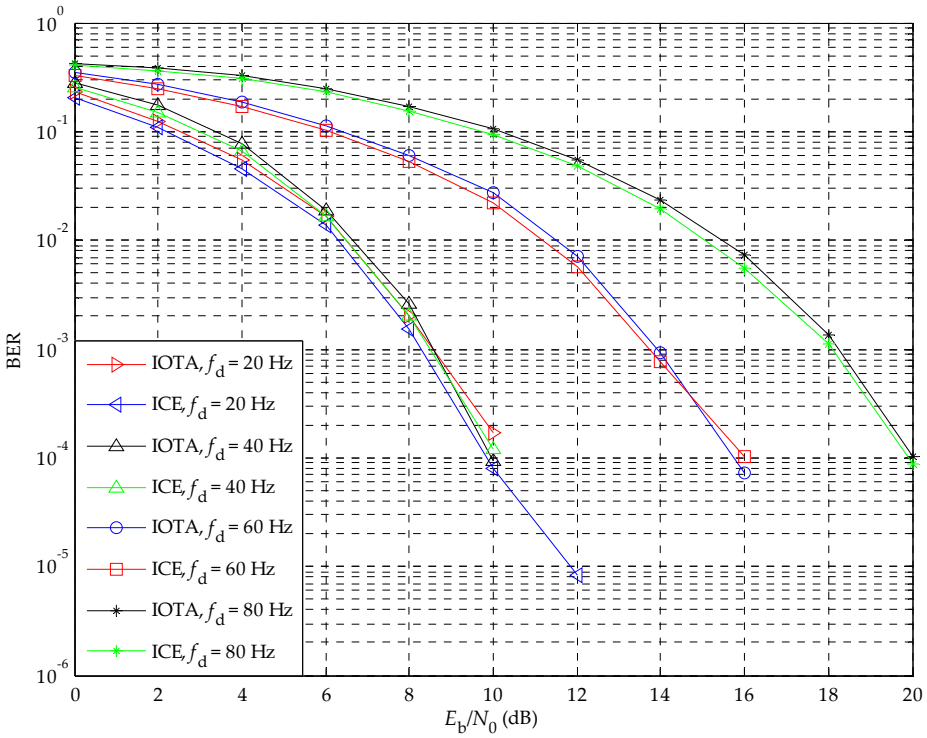


**Figure 4.** Bit error rate (BER) performance of the OFDM/OQPSK system over Rayleigh fading channels with Doppler spread of 20, 40, 60, and 80 Hz. ICE: ideal channel estimation.

The accuracy of channel estimation can be evaluated by the NMSE, which is expressed as:

$$\text{NMSE} = \sqrt{\sum_{n=0}^{N-1} \left| \hat{\boldsymbol{h}}_{m,n} - \boldsymbol{h}_{m,n}^{\text{ICE}} \right|^2 / \sum_{n=0}^{N-1} \left| \boldsymbol{h}_{m,n}^{\text{ICE}} \right|^2}, \tag{9}$$

where $\boldsymbol{h}_{m,n}^{\text{ICE}}$ is the ICE result on the $m$-th subcarrier of the $n$-th OFDM/OQPSK symbol which can be obtained under the condition of no AWGN. $\hat{\boldsymbol{h}}_{m,n}$ is the estimated CIR for the IOTA filter method on the $m$-th subcarrier of the $n$-th OFDM/OQPSK symbol.

Figure 5 illustrates the NMSE versus $E_b/N_0$ for the proposed OFDM/OQPSK system over Rayleigh fading channels with different Doppler spread. The figure shows that the accuracy of channel estimation can be greatly improved when the value of Doppler spread decreased. As shown in Figure 5, when the NMSE value is 0.1, the $E_b/N_0$ gaps between the NMSE performance curves of proposed IOTA filter method with Doppler spread of 20, 40, 60, and 80 Hz are about 0.8, 3.2, and 4.5 dB, respectively. The NMSE simulation results verify that IOTA filter has good orthogonality properties in time and frequency domains, which can be utilized as a wavelet platform in the proposed OFDM/OQPSK system.

### *5.2. The Performance of the OFDM/QPSK System*

The BER performance of the OFDM/QPSK system over Rayleigh fading channels with different Doppler spread is presented in Figure 6. The OFDM/QPSK system adopts comb-type pilots insertion for perfect channel estimation. At the target BER of $10^{-3}$, the $E_b/N_0$ gaps of the LS method under Doppler spread of 20, 40, 60, and 80 Hz are about 8.5, 2.0, and 0.5 dB. Moreover, the $E_b/N_0$ gaps between the BER performance curves of ICE method with Doppler spread of 20, 40, 60, and 80 Hz are about 7.0, 2.2, and 0.8 dB at the target BER of $10^{-4}$.

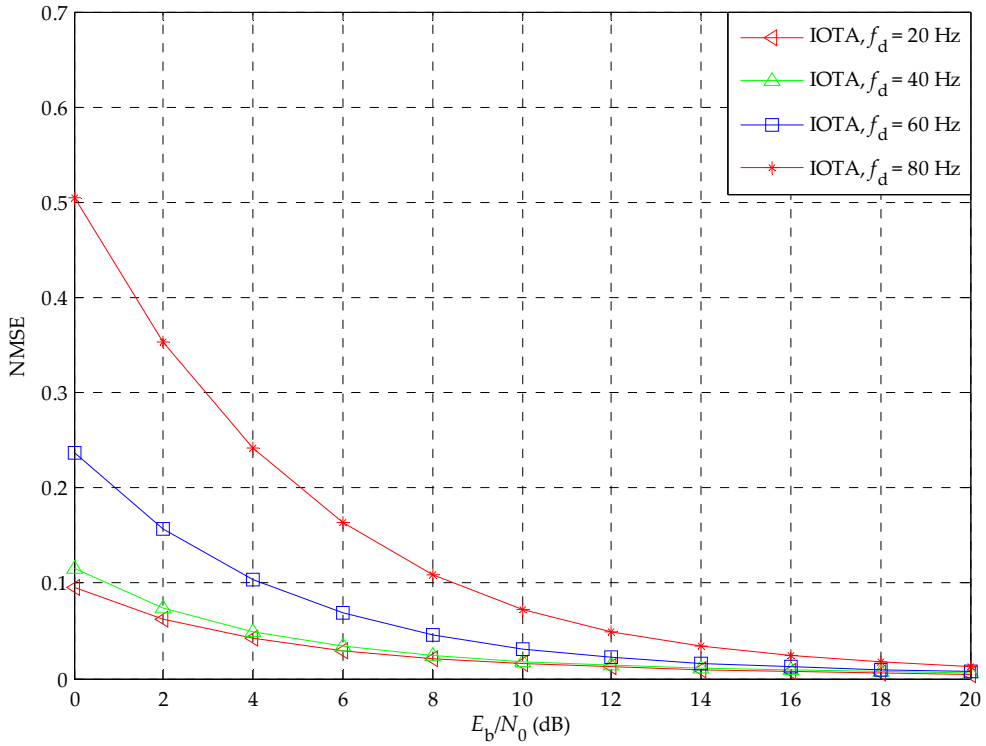


**Figure 5.** Normalized minimum square error (NMSE) performance of the OFDM/OQPSK system over Rayleigh fading channels with Doppler spread of 20, 40, 60, and 80 Hz.

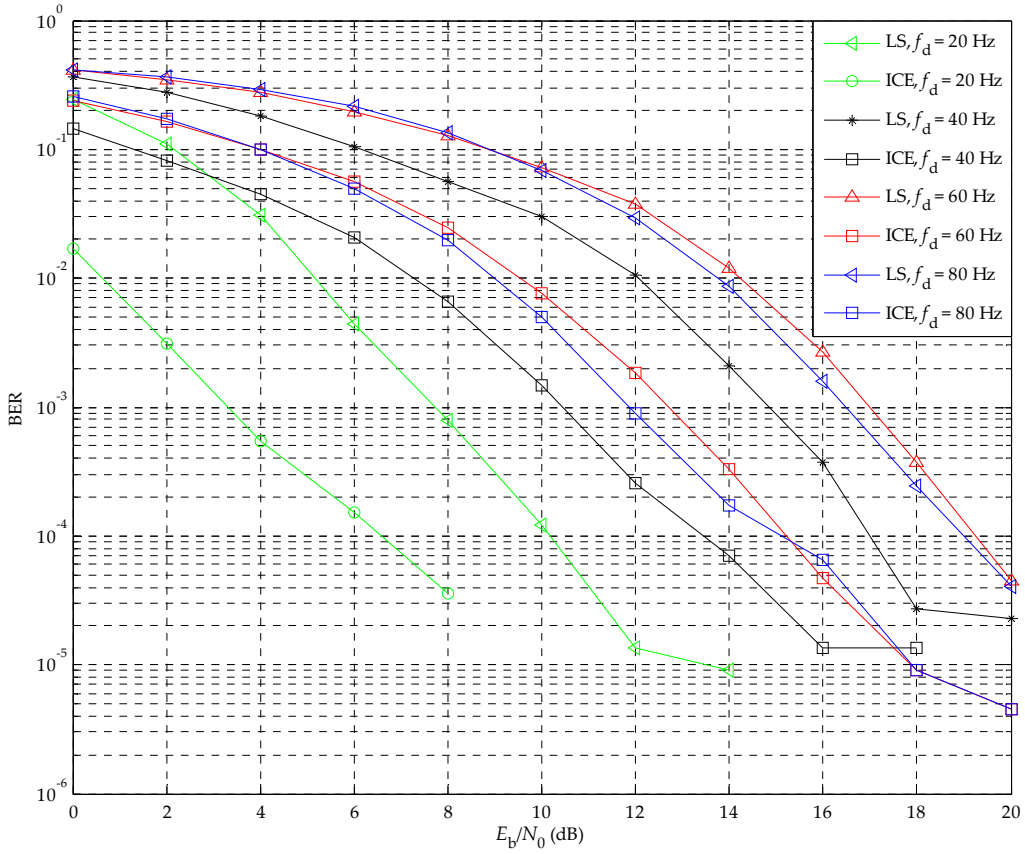


**Figure 6.** BER performance of the OFDM/QPSK system over Rayleigh fading channels with Doppler spread of 20, 40, 60, and 80 Hz. LS: least square.

Figure 7 presents the NMSE performance of the OFDM/QPSK system over Rayleigh fading channels with different Doppler spread, which can be seen is that the LS method with $f_d = 20$Hz outperforms the LS method with $f_d = 40$Hz, $f_d = 60$Hz, and $f_d = 80$Hz by about 4.0, 6.0, and 6.1 dB $E_b/N_0$ gains at the NMSE of 0.1. As shown in Figure 7, the LS method has very low NMSE value with the increase of $E_b/N_0$. It can suppress the AWGN impact and improve the accuracy of the estimated CIR, thereby it can increase the accuracy of channel estimation.

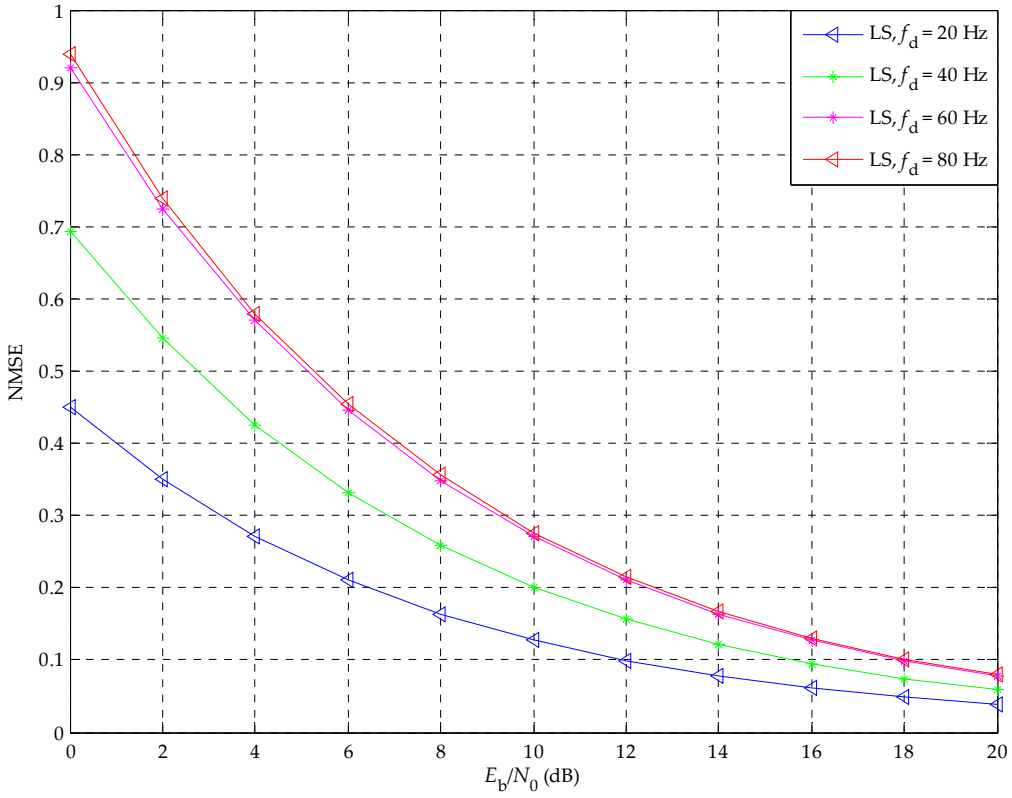


**Figure 7.** NMSE performance of the OFDM/QPSK system over Rayleigh fading channels with Doppler spread of 20, 40, 60, and 80 Hz.

### *5.3. The Performance of the OFDM/OQAM System*

Figure 8 illustrates the BER performance of the proposed OFDM/OQAM system over Rayleigh fading channels with different Doppler spread. As shown in Figure 8, when the maximum Doppler spread increased from 20 Hz to 60 Hz, the proposed IOTA filter method demonstrates its advantage in tracking the channel variation. The BER curve gaps between the IOTA filter method with Doppler spread of 20, 40, and 80 Hz are about 1.8 and 3.5 dB at the target BER of $10^{-4}$. In addition, the BER curve gaps between the ICE method with Doppler spread of 20, 40, and 80 Hz are about 2.0 and 3.1 dB at the target BER of $10^{-4}$. The BER curves under Doppler spread of 40 and 60 Hz are very similar and the BER curves declined rapidly as the $E_b/N_0$ increased. It can be seen that AWGN is the main factor affecting the accuracy of channel estimation in the lower $E_b/N_0$ zone, but the IOTA filter can maintain orthogonality between subcarriers to counteract Rayleigh fading.

Figure 9 presents the NMSE performance of the OFDM/OQAM system over Rayleigh fading channels with different Doppler spread. As shown in Figure 9, the channel estimation results can be accurately measured by the NMSE values. When the NMSE value is 0.02, the $E_b/N_0$ gaps between the NMSE performance curves of the proposed IOTA filter method with the Doppler spread of 20, 40, and 80 Hz are about 1.5 and 4.0 dB, respectively. The IOTA filter is a good choice that can be well adopted in the proposed OFDM/OQAM system. Under the maximum Doppler spread of 40 and 60 Hz, the NMSE curves almost overlap, but the IOTA method with a Doppler spread of 40 Hz still outperforms the Doppler spread of 60 Hz by about 0.03 dB.

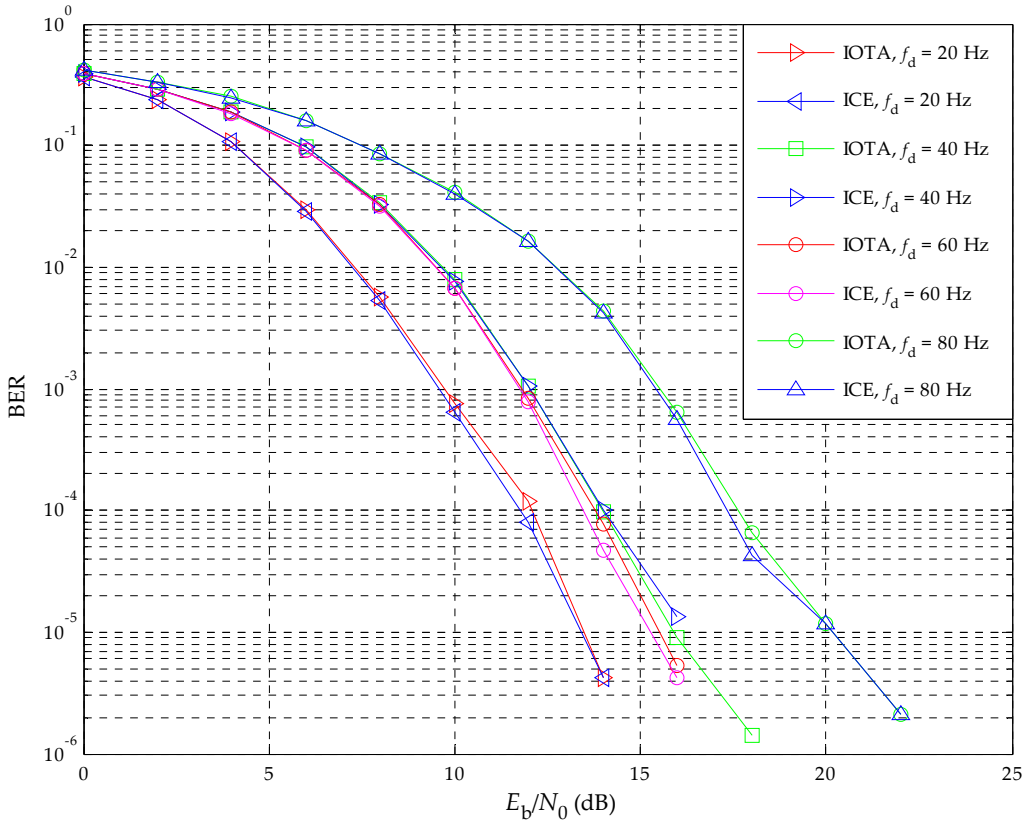


**Figure 8.** BER performance of the OFDM/OQAM system over Rayleigh fading channels with Doppler spread of 20, 40, 60, and 80 Hz.

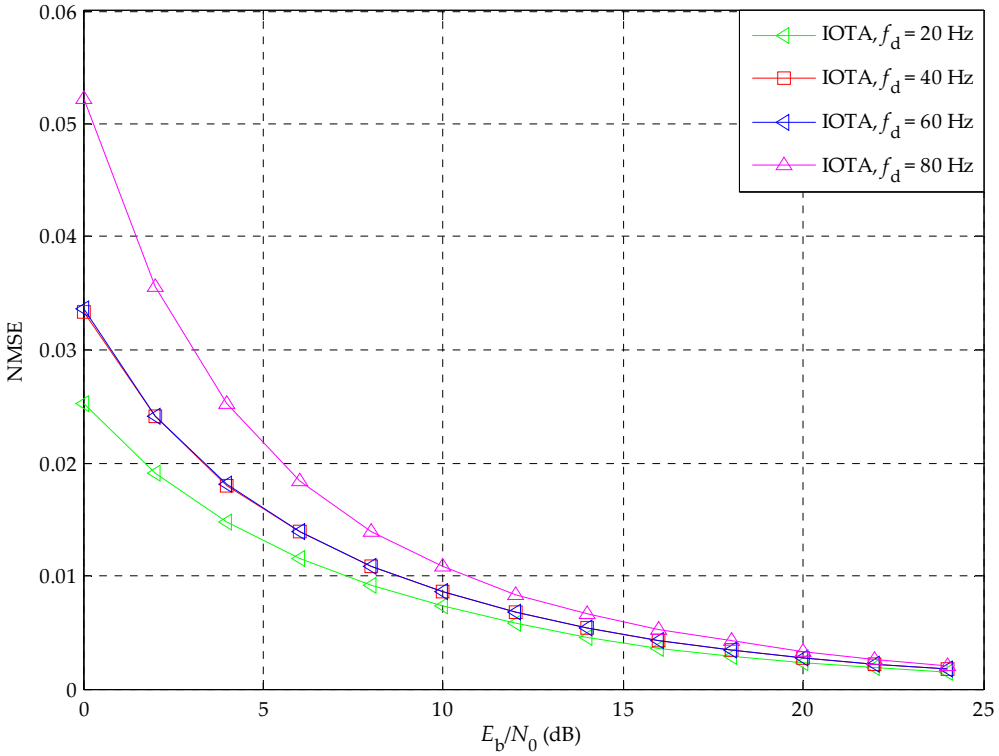


**Figure 9.** NMSE performance of the OFDM/OQAM system over Rayleigh fading channels with Doppler spread of 20, 40, 60, and 80 Hz.

### *5.4. The Performance of the OFDM/16-QAM System*

Figure 10 illustrates the BER performance of OFDM/16-QAM system over Rayleigh fading channels with different Doppler spread. The OFDM/16-QAM system uses comb-type pilots insertion to estimate the CFR. Compared with the ICE method under $f_d = 20$Hz, the ICE method with Doppler spread of 40, 60, and 80 Hz has $E_b/N_0$ degradation about 2.0, 8.0, and 10.5 dB at the target BER of $10^{-3}$. At the target BER of $2 \times 10^{-3}$, the LS method under Doppler spread of 20 Hz provides 1.6, 7.6, and 9.7 dB $E_b/N_0$ gains compared with the LS method under Doppler spread 40, 60, and 80 Hz.

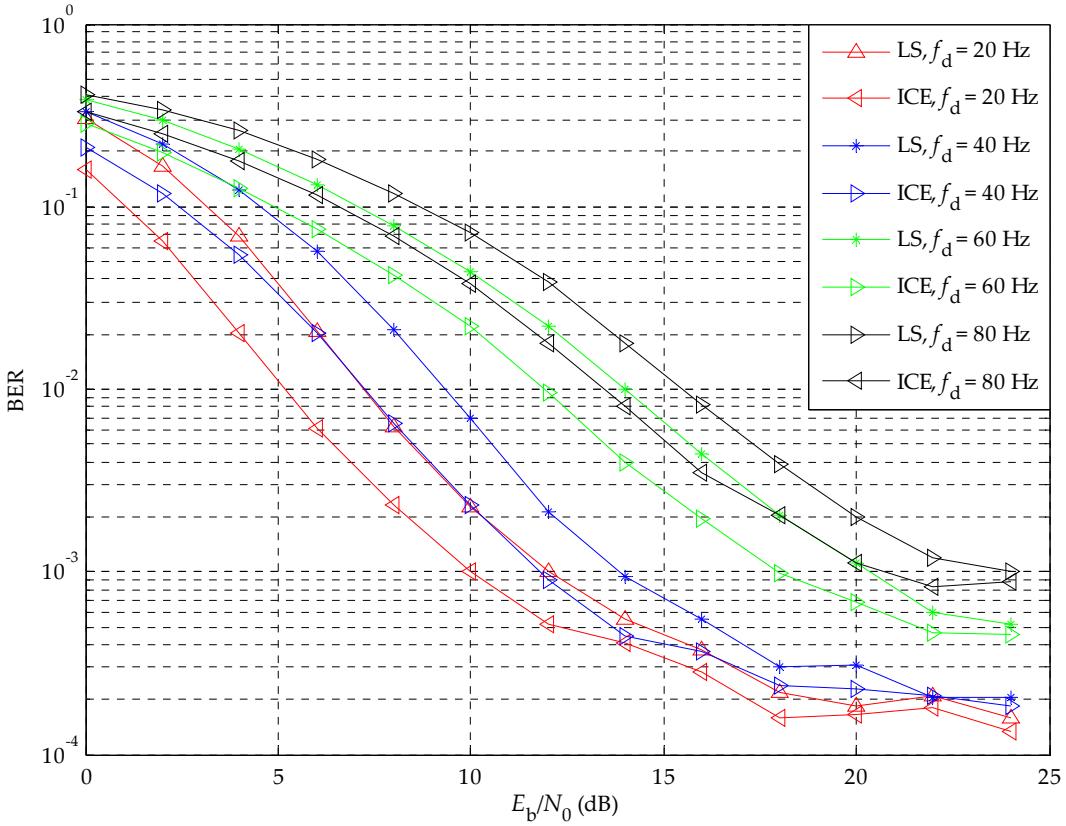


**Figure 10.** BER performance of OFDM/16-QAM system over Rayleigh fading channels with Doppler spread of 20, 40, 60, and 80 Hz.

Figure 11 illustrates the NMSE performance of the OFDM/16-QAM system over Rayleigh fading channels with different Doppler spread. When the NMSE value is 0.05, the LS method with Doppler spread of 20 Hz outperforms the LS method with Doppler spread of 40, 60, and 80 Hz by about 1.0, 3.0, and 5.0 dB $E_b/N_0$ gains. Based on the simulation results of the OFDM/OQAM system and the OFDM/16-QAM system with comb-type pilot insertion, the OFDM/OQAM system enhances the accuracy of channel estimation significantly when it utilizes the NMSE value as the measurement.

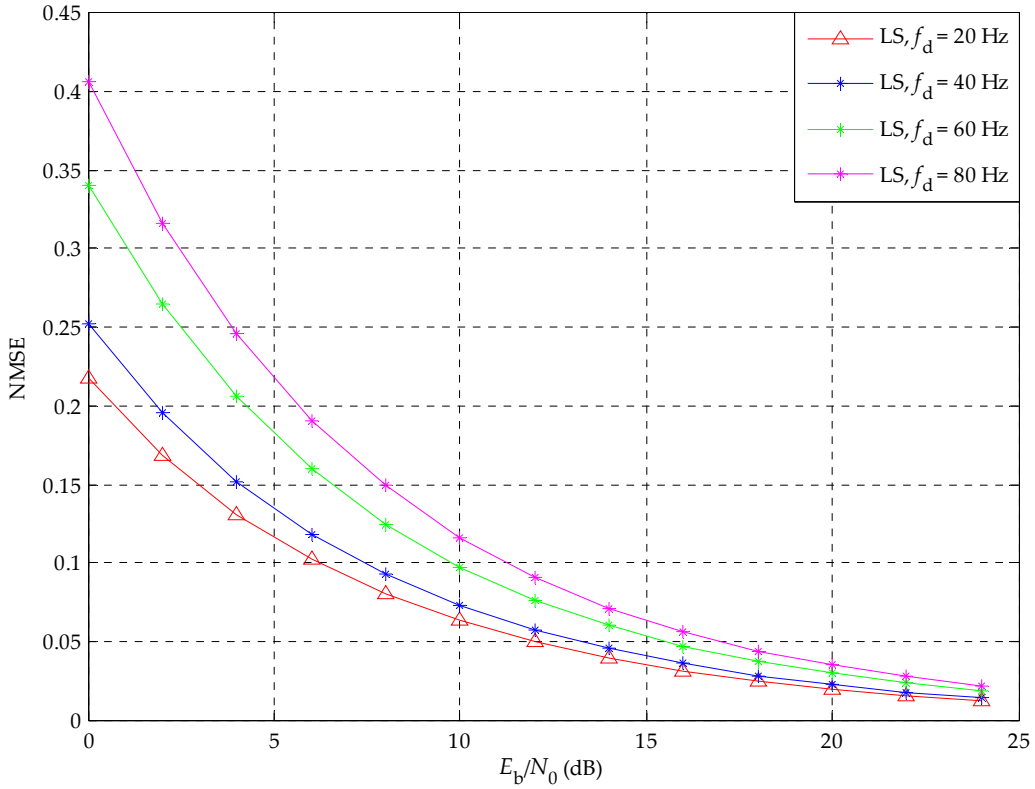


**Figure 11.** NMSE performance of the OFDM/16-QAM system over Rayleigh fading channels with Doppler spread of 20, 40, 60, and 80 Hz.

## 6. Conclusions

This paper proposes a novel channel estimation method based on IOTA filter in OFDM/OQPSK and OFDM/OQAM systems. The channel estimation method provides a high data transmission rate and spectral efficiency while the IOTA wavelet can suppress the AWGN existing at the estimated CIRs of the OFDM receiver. Simulation results verify that the channel estimation method provides good BER and NMSE performance under both static and dynamic frequency-selective channels. The IOTA filter can guarantee orthogonality between different subcarriers and suppress the ICI efficiently in the frequency domain. Meanwhile, the IOTA filter reduces the ISI among consecutive OFDM frames in the time domain and reduces the BER significantly. The channel encoder and channel decoder are adopted to provide robust channel estimation against AWGN in both OFDM-IOTA and CP-OFDM systems.

Compared with ICE and LS channel estimation methods, the proposed channel estimation method has better performance. The IOTA filter not only provides better performance but also has high data transmission rate and spectral efficiency since it does not require GI in front of each OFDM frame. With the improvement of the fifth-generation (5G) technology, there are more demands for high transmission data rate and spectral efficiency in wireless communication systems. Therefore, the proposed IOTA filter channel estimation method has broad software and hardware application prospects and can be utilized in ultra-wideband (UWB) OFDM communication systems [18–20], optical communication systems, and OFDM time division dual (TDD) communication systems [21–23].

In the future, we will compare IOTA wavelet with other wavelets for channel estimation in OFDM systems. We will make a better adoption of radio frequency filtering technology in frequency-selective and dynamic channels.

**Author Contributions:** X.Z. and C.W. conceived the algorithm and designed the experiments; X.Z. and R.T. performed the experiments; X.Z. and C.W. analyzed the results; X.Z. drafted the manuscript; X.Z., C.W., and R.T. revised the manuscript. All authors read and approved the final manuscript.

**Funding:** This work was supported by the National Natural Science Foundation of China (No. 61702303) and the Shandong Provincial Natural Science Foundation, China (No. ZR2017MF020).

**Conflicts of Interest:** The authors declare no conflict of interest.

## References

1. Galande, N.A.; Shah, A.M. Implementation of OFDM by using wavelet for optimization of wireless communication system. In Proceedings of the IEEE International Conference on Recent Trends in Electronics, Information and Communication Technology, Bangalore, India, 20–21 May 2016; pp. 451–455. [CrossRef]
2. Du, J.F.; Signell, S. Time frequency localization of pulse shaping filters in OFDM/OQAM systems. In Proceedings of the 6th International Conference on Information, Communications and Signal Processing, Singapore, Singapore, 10–13 December 2007; pp. 1–5. [CrossRef]
3. Sheela, M.S.; Surekha, T.P.; Arjun, K.R. Analysis of BER in OFDM using wavelet and FFT based method. In Proceedings of the International Conference on Current Trends in Computer, Electrical, Electronics and Communication, Mysore, India, 8–9 September 2017; pp. 473–476. [CrossRef]
4. Yoo, T.W.; Im, S.B.; Hwang, S.H.; Choi, H.J. Pilot structure for high data rate in OFDM/OQAM-IOTA system. In Proceedings of the 68th IEEE Vehicular Technology Conference, Calgary, AB, Canada, 21–24 September 2008; pp. 1–5. [CrossRef]
5. Kongara, K.P.; Smith, P.J.; Mann, S. A comparison of CP-OFDM with IOTA-OFDM under typical system imperfections. In Proceedings of the IET Seminar on Wideband and Ultrawideband Systems and Technologies, London, UK, 6 November 2008; pp. 1–5. [CrossRef]
6. Mehmood, S.; Dasalukunte, D.; Öwall, V. Hardware architecture of IOTA pulse shaping filters for multicarrier systems. *IEEE Trans. Circuits Syst. Regul. Pap.* **2013**, *60*, 733–742. [CrossRef]
7. Du, J.; Xiao, P.; Wu, J.; Chen, Q. Design of isotropic orthogonal transform algorithm based multicarrier systems with blind channel estimation. *IET Commun.* **2012**, *6*, 2695–2704. [CrossRef]
8. Kurt, T.; Siala, M.; Yongaçoglu, A. Multi-carrier signal shaping employing Hermite functions. In Proceedings of the 13th European Signal Processing Conference, Antalya, Turkey, 4–8 September 2005; pp. 2026–2029.
9. Razavi, R.; Xiao, P.; Tafazolli, R. Information theoretic analysis of OFDM/OQAM with utilized intrinsic interference. *IEEE Signal Process. Lett.* **2015**, *22*, 618–622. [CrossRef]
10. Kol, V.K.; Mishra, A. Discrete wavelet transform based OFDM-IDMA system with AWGN channel. In Proceedings of the Students Conference on Engineering and Systems, Allahabad, India, 12–14 April 2013; pp. 1–4. [CrossRef]
11. Abdullah, K.; Al-Hinai, N.; Sadik, A.Z.; Hussain, Z.M. Circular 16-QAM modulation scheme for wavelet and Fourier based OFDM systems. In Proceedings of the 5th GCC Conference and Exhibition, Kuwait City, Kuwait, 17–19 March 2009; pp. 1–5. [CrossRef]
12. Bader, F.; Shaat, M.; Medjahdi, Y. New opportunities for spectrum coexistence using advanced multicarrier scheme. In Proceedings of the Military Communications and Information Systems Conference, Saint Malo, France, 7–9 October 2013; pp. 1–6.
13. Suma, M.N.; Narasimhan, S.V.; Kanmani, B. The OFDM system based on discrete cosine harmonic wavelet transform. In Proceedings of the National Conference on Communications, Kharagpur, India, 3–5 February 2012; pp. 1–5. [CrossRef]
14. Siohan, P.; Roche, C. Cosine-modulated filterbanks based on extended Gaussian functions. *IEEE Trans. Signal Process.* **2000**, *48*, 3052–3061. [CrossRef]
15. Zhou, X.; Ye, Z.; Liu, X.X.; Wang, C.Y. Channel estimation based on linear filtering least square in OFDM systems. *J. Commun.* **2016**, *11*, 1005–1011. [CrossRef]
16. Zhou, X.; Ye, Z.; Liu, X.X.; Wang, C.Y. Chi-square distribution-based confidence measure channel estimation method in OFDM Systems. *IETE J. Res.* **2017**, *63*, 662–670. [CrossRef]
17. Jacob, N.; Sripati, U. Bit error rate of coded OFDM for digital audio broadcasting system, employing parallel concatenated convolutional turbo codes. In Proceedings of the IEEE International Conference on Signal Processing, Informatics, Communication and Energy Systems, Calicut, India, 19–21 February 2015; pp. 1–5. [CrossRef]

18. Verma, S.; Sharma, P.; Ahuja, S.; Hajela, P. Partial transmit sequence with convolutional codes for reducing the PAPR of the OFDM signal. In Proceedings of the 3rd International Conference on Electronics Computer Technology, Kanyakumari, India, 8–10 April 2011; pp. 70–73. [CrossRef]
19. Khan, K.; Sheikh, S.A. PAPR reduction of OFDM signals using convolutional codes. In Proceedings of the IEEE Student Conference on Research and Development, Serdang, Malaysia, 16–18 November 2009; pp. 26–28. [CrossRef]
20. Ahmad, N.; S-Yusof, S.K.; Fisal, N. Analysis of recursive systematic convolutional turbo codes in MB-OFDM UWB with channel estimation. In Proceedings of the International Conference on Computer Applications and Industrial Electronics, Kuala Lumpur, Malaysia, 5–8 December 2010; pp. 137–141. [CrossRef]
21. Cho, S.C.; Kim, J.U.; Lee, K.T.; Cho, K.R. Convolutional turbo coded OFDM/TDD mobile communication system for high speed multimedia services. In Proceedings of the Advanced Industrial Conference on Telecommunications/Service Assurance with Partial and Intermittent Resources Conference/E-Learning on Telecommunications Workshop, Lisbon, Portugal, 17–20 July 2005; pp. 244–248. [CrossRef]
22. Tang, R.G.; Zhou, X.; Wang, C.Y. A Haar wavelet decision feedback channel estimation method in OFDM systems. *Appl. Sci.* **2018**, *8*, 877. [CrossRef]
23. Ben Mabrouk, M.; Chafii, M.; Louet, Y.; Bader, F. Low-PAPR condition for 5G-candidate waveforms. In Proceedings of the General Assembly and Scientific Symposium of the International Union of Radio Science, Montreal, QC, Canada, 19–26 August 2017; pp. 1–4. [CrossRef]